Applied Catalysis B: Environmental 150–151 (2014) 82–92

Contents lists available at ScienceDirect

Applied Catalysis B: Environmental

journal homepage: www.elsevier.com/locate/apcatb

Catalytic performance and characterization of Co/Mg/Al catalysts prepared from hydrotalcite-like precursors for the steam gasification of biomass

Lei Wang[a], Dalin Li[a,b], Hideo Watanabe[c], Masazumi Tamura[a], Yoshinao Nakagawa[a], Keiichi Tomishige[a,*]

[a] Department of Applied Chemistry, School of Engineering, Tohoku University, 6-6-07, Aoba, Aramaki, Aoba-ku, Sendai 980-8579, Japan
[b] National Engineering Research Center of Chemical Fertilizer Catalyst, College of Chemistry and Chemical Engineering, Fuzhou University, Gongye Road 523, Fuzhou, Fujian 350002, PR China
[c] Graduate School of Pure and Applied Sciences, University of Tsukuba, 1-1-1, Tennodai, Tsukuba, Ibaraki 305-8573, Japan

ARTICLE INFO

Article history:
Received 24 October 2013
Received in revised form
27 November 2013
Accepted 3 December 2013
Available online 8 December 2013

Keywords:
Cobalt
Hydrotalcite
Steam gasification
Biomass
Tar

ABSTRACT

The Co/Mg/Al catalysts were prepared from the hydrotalcite-like compounds containing Co, Mg and Al, and applied to the steam gasification of biomass. It is found that the Co/Mg/Al (10/40/50) catalyst exhibited much higher activity and resistance to coke deposition than Co/α-Al_2O_3, Co/Al, Co/Mg and Ni/Mg/Al (9/66/25) catalysts. The catalyst characterization using BET, TPR, TPO, XRD, H_2 adsorption, and TEM indicates that the Co/Mg/Al (10/40/50) catalyst after the reduction has a nanocomposite structure of Co metal particles (~14 nm) and oxide particles (~16 nm) of $MgAl_2O_4$-based solid solution. On the other hand, according to the catalyst characterization after the catalytic use and regeneration, the structural change of $MgAl_2O_4$-based solid solution to MgO-based solid solution can be a cause of the decrease of the catalytic activity.

1. Introduction

Conversion of biomass to hydrogen and synthesis gas is an important process for the production of renewable fuels and chemicals from biomass [1–3]. This is because synthesis gas is converted to liquid fuels and chemicals such as hydrocarbons by Fischer–Tropsch synthesis, methanol and so on [1,4–6], and hydrogen is a promising energy carrier combined with the fuel cell technology. High reaction temperature has been applied in the non-catalytic gasification in order to decrease the tar amount, however high temperature is unfavorable in terms of the energy efficiency [4]. In order to enhance the energy efficiency, the decrease in the gasification temperature has been attempted by the utilization of catalysts [7–9]. One of effective methods is metal-catalyzed steam reforming and partial oxidation [10–25] of the biomass tar or bio-oil, and biomass-related compounds. In particular, the development of the Ni-based catalysts for the gasification of wood biomass has been carried out recently, for example, nano-NiO/γ-Al_2O_3 and nano-Ni–La–Fe/Al_2O_3 by Li et al. [26], NiO–MgO solid solution catalyst by Wang et al. [27], NiO-loaded calcined dolomite catalysts by Corujo et al. [28], supported Ni catalysts promoted by various modifiers has also been developed [29–46].

On the other hand, supported Co catalysts also have been utilized to the steam gasification of biomass [47–50] and steam reforming of its model compounds such as naphthalene [10,51], toluene [36,52], ethanol [53–55], methanol [56], acetic acid [57] and so on.

It has been known that the metal catalysis in the steam reforming of hydrocarbon and oxygenates can be affected by the interaction of metal species with support surfaces and modifiers. One possible method to increase the interaction between metals and oxide supports is the preparation of catalysts using hydrotalcite-like compounds as a precursor [58,59]. One of the typical hydrotalcite-like compounds is layered double hydroxides (LDHs), which are a class of lamellar compounds that consist of positively charged brucite-like host layers and hydrated exchangeable anions located in the interlayer gallery for charge balance [58]. The charge of the brucite-like layers arises from the isomorphous substitution of a part of the divalent metal ions with trivalent ones. The chemical composition of LDHs are expressed by the general formula $[M^{II}_{1-x}M^{III}_x(OH)_2][A^{n-}_{x/n}\cdot mH_2O]$, where M^{II} and M^{III}

* Corresponding author. Tel.: +81 22 795 7214; fax: +81 22 795 7214.
E-mail addresses: tomi@erec.che.tohoku.ac.jp, tomi@tulip.sannet.ne.jp (K. Tomishige).

0926-3373/$ – see front matter © 2013 Elsevier B.V. All rights reserved.
http://dx.doi.org/10.1016/j.apcatb.2013.12.002

represent di- and trivalent metal ions inside the brucite-like layers, and A^{n-} is an interlayer anion [58,60–65]. In addition, the calcination of the hydrotalcite-like compounds gives mixed oxides that exhibit some significant properties such as large surface area, high thermal stability, high dispersion, and basic character [58]. Moreover, the subsequent reduction of the calcined samples containing reducible metal ions gives well-dispersed and thermally stable metal particles [58]. Based on these reasons, the hydrotalcite-like materials have been the subject of intense research because of their wide applications as catalysts and catalyst precursors [58,66,67]. It has been reported that the calcination followed by the reduction of hydrotalcite-like compounds containing Ni species gave the nano-composite of Ni metal particles and Mg(Ni, Al)O with comparable size (~10 nm). The nano-composite catalyst exhibited much higher catalytic performance in the steam gasification of cedar wood in terms of the catalytic activity and the suppression of the coke formation than the conventional supported Ni catalysts [35,59].

It has also been reported that Co catalysts derived from hydrotalcite-like compounds were effective to various catalytic reaction like ethanol steam reforming [68,69], glycerol hydrogenolysis [70], NO_x and N_2O removal [71–74], hydrocarbon oxidation [75–77] and so on.

In this article, a series of Co/Mg/Al catalysts were prepared from hydrotalcite-like compounds as precursors. They were characterized by means of BET, XRD, temperature programmed reduction (TPR), temperature programmed oxidation (TPO), the measurement of BET surface area, H_2 adsorption and TEM. Their catalytic performance in the steam gasification of biomass was evaluated and compared with that of conventional Co/α-Al_2O_3 and the Ni catalyst prepared by using the hydrotalcite-like compounds. The superiority of the optimized Co catalyst prepared by using the hydrotalcite-like compounds was also demonstrated comparing with the optimized Ni/Mg/Al prepared in the similar way [59].

2. Experimental

2.1. Catalyst preparation

Hydrotalcite-like compounds containing Co were prepared by coprecipitation of the nitrates of metal components on the basis of the previous report [60] with minor modifications. The mixed aqueous solution of $Mg(NO_3)_2{\cdot}6H_2O$ (Wako), $Al(NO_3)_3{\cdot}9H_2O$ (Wako) and $Co(NO_3)_2{\cdot}6H_2O$ (Wako) was added slowly into a beaker containing an aqueous solution of sodium carbonate under stirring at room temperature and a constant pH of 10 ± 0.5. The pH of the solution was adjusted with an aqueous solution of sodium hydroxide (2 M). The resulting suspension was then kept at room temperature for 24 h. The resulting precipitate was filtered and washed several times with de-ionized water and dried at 383 K for one night. The precipitate was ground to fine powders and then calcined at 1073 K for 5 h in a static air atmosphere. The obtained material was pressed to a disk, crushed and sieved to particles with 30–60 mesh size (0.3–0.6 mm), and the resulting material as denoted as Co/Mg/Al. The composition of Co/Mg/Al samples prepared in this work is listed in Table 1. The Co content of Co/Mg/Al catalyst is 12 wt% as a weight percentage. The catalysts are denoted as Co/Mg/Al (x/y/z), where x, y, and z represented the atomic percentage of Co, Mg, and Al, respectively. For comparison, Co/Mg, Co/Al and Ni/Mg/Al (9/66/25) [59] samples were also prepared by co-precipitation of the nitrates of corresponding metal components, followed by drying and calcination at 1073 K for 5 h.

For Co/α-Al_2O_3 catalyst, the support material of α-Al_2O_3 was prepared by the calcination of γ-Al_2O_3 (KHO-24, Sumitomo Chemical Co., Ltd, 133 m^2/g, grain size 2–3 mm) in air at 1423 K. After the calcination, it was crushed and sieved to particle sizes between 0.3 and 0.6 mm. The Co/α-Al_2O_3 catalyst was prepared by a impregnation method using the aqueous solution of $Co(NO_3)_2{\cdot}6H_2O$ (Wako). After the impregnation, the sample was dried at 383 K for 12 h followed by the calcination at 773 K for 3 h under air atmosphere, and the loading amount of Co was 12 wt%, and the BET surface area was determined to be 10 m^2/g.

2.2. Activity test in the steam gasification of cedar wood

Cedar wood was ground with a ball mill to about 0.1–0.3 mm size. The moisture content of the cedar wood was 7.2%. The dry-based composition by weight was C 50.8%, H 6.0%, O 41.8%, N 0.2%, and ash 1.1%. The elemental analysis was carried out by the Japan Institute of Energy.

Catalytic performance was evaluated using a laboratory-scale continuous feeding dual-bed reactor that was described in our previous report [30], and the details of the procedure for catalytic performance evaluation in the steam gasification of biomass have been also described [30]. In this reactor, the biomass particles were fed to the primary bed for the biomass pyrolysis continuously at the constant rate (the feeding rate of biomass: 60 mg/min, and the feeding rate of C, H, and O was 2360, 3350 and 1450 μmol/min, respectively, excluding the moisture content). Together with N_2 carrier gas (60 ml/min, 2680 μmol/min), steam was also supplied to the reactor by the evaporation of water fed by a syringe pump (555–1110 μmol/min). The molar ratio of the feeding steam to feeding carbon in the biomass was denoted as S/C, and the conditions of S/C = 0.23–0.47 were applied. The molar ratio of the total steam (the feeding steam + the moisture in the biomass) to feeding carbon in the biomass was calculated to be 0.34–0.57.

The tests were performed under atmospheric pressure by using 0.3 g of catalyst. Co/Mg/Al and Ni/Mg/Al catalysts were reduced with H_2/N_2 (30/30 ml/min) mixed gas at 1073 K for 0.5 h before the activity test [59]. The Co/α-Al_2O_3 catalyst was reduced at 773 K for 0.5 h using 30 ml/min H_2 before the activity test [36,50]. The test for the evaluation of the catalytic activity started with the biomass feeding and continued for 15 min. The formation rate of gaseous products was almost constant during 15 min on all the tested catalysts. During the test, the effluent gas was collected by a syringe and the flow rate of the gas was measured by a bubble meter. The collected gas was analyzed by gas chromatograph (GC). The concentration of CO, CO_2, and CH_4 was measured by FID-GC equipped with a methanator and that of H_2 was determined by TCD-GC. The yield of CO, CO_2 and CH_4 is calculated by the formation rate and the reaction time normalized by the total carbon supplying rate of the biomass. After the activity test for 15 min, the amount of char accumulated in the primary bed and the amount of coke deposited on the catalyst surface were measured by the amount of CO_2 formed by the combustion when the O_2 was fed at 873 K, and the yield of char and coke was calculated by the ratio to the total carbon amount in the fed biomass. As a result, the yield of gaseous products and solid products (coke and char) were determined. On the other hand, tar is so condensable in the reactor systems that the amount of residual tar is difficult to determine precisely. Therefore, the yield of tar is obtained by the subtraction of carbon-based yield of gaseous and solid products from the total. In the present experiments, the amount of the tar condensed in the reactor systems was not so large that the tar did not plug the pass of the effluent gas even in the test for the longer reaction time. In addition, the formation rate of $CO + H_2$ was also plotted in the results as a desired product in the steam gasification. In order to evaluate the catalyst stability, the longer reaction time than 15 min and the regeneration of the deactivated catalysts were adopted. In particular, after the test for a specific time, the used catalysts were oxidized in O_2/N_2 (1/3) at 873 K for 60 min, and reduced subsequently in H_2/N_2 (1/1) at 1073 K for 30 min, for the catalyst regeneration. After these regeneration procedures, the catalysts were used for the activity test again.

Table 1
Composition of Co/Mg/Al and Ni/Mg/Al catalysts.

Catalysts	Atomic percentage			(Co + Mg)/Al or (Ni + Mg)/Al atomic ratio
	Co or Ni	Mg	Al	
Co/Al	11	–	89	–
Co/Mg/Al (10/10/80)	10	10	80	0.25
Co/Mg/Al (10/23/67)	10	23	67	0.5
Co/Mg/Al (10/40/50)	10	40	50	1
Co/Mg/Al (9/57/33)	9	57	33	2
Co/Mg/Al (9/66/25)	9	66	25	3
Co/Mg/Al (9/74/17)	9	74	17	5
Co/Mg	9	91	–	–
Ni/Mg/Al (9/66/25)	9	66	25	3

2.3. Catalyst characterization

The surface area was measured by BET method using Gemini 2360 Micromeritics.

Temperature-programmed reduction (TPR) with H_2 was performed in the fixed-bed flow reactor. The TPR profile of each sample was recorded from room temperature to 1273 K under a flow of 5.0% H_2/Ar, and the flow rate was 30 ml/min. The catalyst weight was 50 mg. The heating rate was 10 K/min and the temperature was maintained at 1273 K for 30 min after it reached 1273 K. The consumption of H_2 was monitored continuously with TCD equipped with frozen acetone trap in order to remove H_2O from the effluent gas. The amount of H_2 consumption was estimated from the peak area in the TPR profiles.

Temperature-programmed oxidation (TPO) with O_2 was also carried out in the fixed-bed flow reactor. Catalyst samples were reduced in H_2/N_2 (30/30 ml/min) mixed gas at 1073 K for 0.5 h in the laboratory-scale continuous feeding dual-bed reactor used for the activity tests and they were transferred to the fixed-bed reactor in the air. The TPO profile of each sample was recorded from room temperature to 1073 K at a heating rate of 10 K/min under a flow of 1.0% O_2/He at the flow rate of 30 ml/min. About 50 mg of the reduced sample was used for the TPO measurement. The consumption of O_2 was monitored continuously with TCD gas chromatograph, and the amount of O_2 consumption was used to calculate the Co reduction degree, assuming that $3Co^0 + 2O_2 \rightarrow Co_3O_4$ [78].

H_2 chemisorption experiments were carried out in a vacuum line by a volumetric method. The catalysts were ex-situ reduced at 1073 K for 0.5 h in H_2/N_2 (30/30 ml/min) mixed gas in the laboratory-scale continuous feeding dual-bed reactor. The sample weight was about 150 mg. Before H_2 adsorption measurement, the catalysts were in-situ treated in H_2 (1 atm) at 773 K for 0.5 h, and evacuated at 773 K in the vacuum line. H_2 adsorption was performed at room temperature. Gas pressure at adsorption equilibrium was about 1.1 kPa. The dead volume of the apparatus was about 60 cm^3. For the estimation of Co metal dispersion, the molar ratio of adsorbed hydrogen atom to the surface Co atom is one on the basis of the previous reports [78,79].

Powder X-ray diffraction (XRD) patterns of the freshly reduced and used catalysts were collected on a Rigaku, MiniFlex 600 using Cu $K\alpha$ (λ = 0.154 nm) generated at 40 kV and 20 mA in air-atmosphere. The average size of Co metal particles on the catalyst was calculated using the Scherrer's equation [80].

Transmission electron microscope (TEM) images were taken by means of the instrument (JEM-2010F, JEOL) operated at 200 kV. The sample powders after the reduction were dispersed in 2-propanol by supersonic wave and put on Cu grids for TEM observation under air. Average particle size was calculated by $\sum n_i d_i^3 / \sum n_i d_i^2$ (d_i: average particle size, n_i: number of particle with d_i) [14].

3. Results and discussion

3.1. Catalyst characterization of fresh catalysts

Fig. 1 shows the XRD patterns of the as-synthesized Co/Mg/Al precursors with varying (Co + Mg)/Al ratios of 0.25–5, together with those of the precursors of Co/Al and Co/Mg. The XRD pattern of the Co/Al precursor gave the phases of AlOOH boehmite [81] mainly (Fig. 1a). On the other hand, all of the Co/Mg/Al precursors exhibited the characteristic peaks of the hydrotalcite-like compounds [82], and the peaks due to the hydrotalcite-like compounds became more clearly from Co/Mg/Al (10/10/80) (Fig. 1b) to Co/Mg/Al (9/57/33) (Fig. 1e). At low (Co + Mg)/Al (≦0.5), the boehmite phase was also detected as a impurity (Fig. 1b).

The hydrotalcite structure, $[Mg_{1-x-y}Co_xAl_y(OH)_2]^{y+}(CO_3)_{y/2}\cdot mH_2O$, consists of layered double hydroxide with brucite structure where Co^{2+}, Mg^{2+} and Al^{3+} cations share octahedral positions. The d-spacing of the (0 0 3) reflection near $2\theta = 11^\circ$ corresponds to the thickness of one layer constituting a brucite-like sheet and one interlayer [58]. The d-spacing increased steadily from 0.75 to 0.80 nm as the (Co + Mg)/Al ratio increased (Fig. 2), which is attributed to the decreased electrostatic interaction between layer and interlayer as the excess charge introduced by the trivalent Al^{3+} ion is decreased. The d-spacing of the (1 1 0) reflection at $2\theta = 60$–61° is related to the average metal–metal distance in the

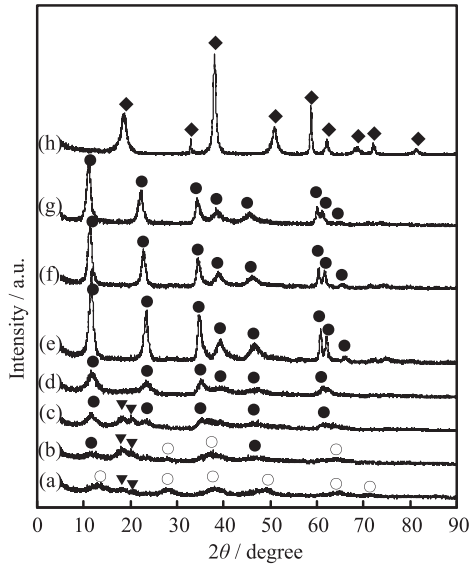

Fig. 1. XRD patterns of the as-synthesized samples: (a) Co/Al, (b) Co/Mg/Al (10/10/80), (c) Co/Mg/Al (10/23/67), (d) Co/Mg/Al (10/40/50), (e) Co/Mg/Al (9/57/33), (f) Co/Mg/Al (9/66/25), (g) Co/Mg/Al (9/74/17) and (h) Co/MgO. ♦ = $Mg(OH)_2$ brucite, ● = Co/Mg/Al hydrotalcite, ○ = AlOOH boehmite and ▼ = $Al(OH)_3$.

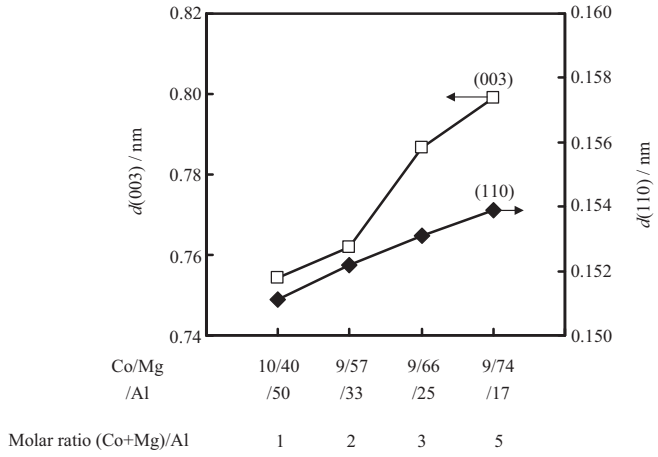

Fig. 2. Variation of XRD peak positions of the (0 0 3) and (1 1 0) reflections as a function of (Co + Mg)/Al molar ratio.

layer [58]. These distances increased with the (Co + Mg)/Al ratio, which is expected to be due to the larger ionic radii of Mg^{2+} and Co^{2+} than that of Al^{3+} (0.072 nm for Mg^{2+}, 0.065 nm for Co^{2+} and 0.054 nm for Al^{3+}) in octahedral coordination [83].

In the XRD pattern of Co/Mg precursor, the diffraction peak at $2\theta = 38.01^\circ$ was slightly shifted to higher diffraction angle in comparison with 37.98° for pure $Mg(OH)_2$ brucite [84], which may also be attributed to the incorporation of Co^{2+} in the $Mg(OH)_2$ structure and the shift of the diffraction angle is due to the smaller ionic radius of Co^{2+} (0.065 nm) than that of Mg^{2+} (0.072 nm).

Fig. 3 shows the XRD patterns of the Co/Mg/Al, Co/Al and Co/Mg after the calcination. In the case of Co/Al, the peaks assigned to $CoAl_2O_4$ spinel [85] were observed. Considering the molar ratio of Co to Al in Co/Al, the residual Al can give a compound with weaker XRD peaks like γ-Al_2O_3.

On the Co/Mg/Al catalysts, the characteristic XRD patterns assigned to hydrotalcite completely disappeared, on Co/Mg/Al ((Co + Mg)/Al < 1), the other phase appeared and it was assigned to $MgAl_2O_4$ spinel [86] instead of $CoAl_2O_4$ spinel (Fig. 3b–e). The

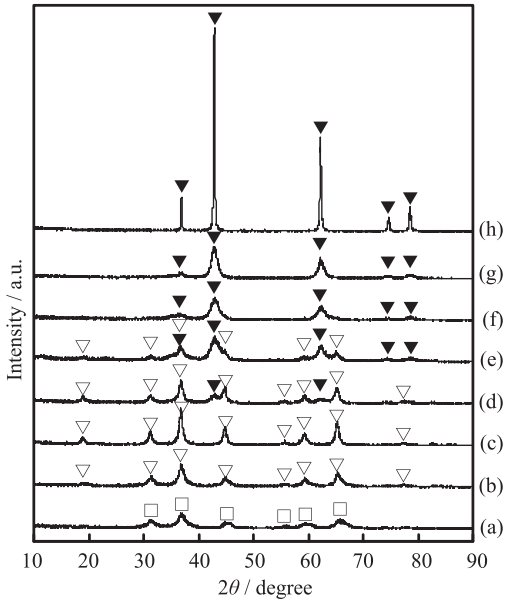

Fig. 3. XRD patterns of the samples after calcination: (a) Co/Al, (b) Co/Mg/Al (10/10/80), (c) Co/Mg/Al (10/23/67), (d) Co/Mg/Al (10/40/50), (e) Co/Mg/Al (9/57/33), (f) Co/Mg/Al (9/66/25), (g) Co/Mg/Al (9/74/17) and (h) Co/MgO. ▼ = MgO-based solid solution, ▽ = $MgAl_2O_4$-based solid solution and □ = $CoAl_2O_4$ spinel.

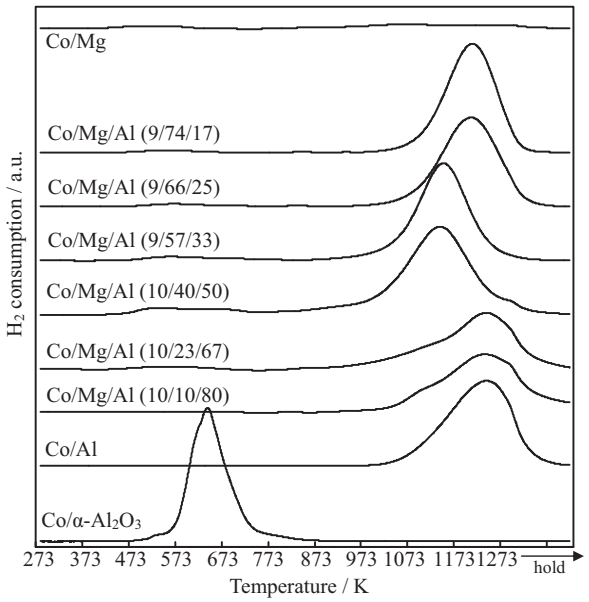

Fig. 4. TPR profiles of Co/Mg, Co/Al and Co/Mg/Al catalysts. TPR conditions: heating rate 10 K/min, 5% H_2/Ar flow rate 30 ml/min. Sample weight: 50 mg.

diffraction pattern of $MgAl_2O_4$ was similar to that of $CoAl_2O_4$. However, the peak at 19.02° is characteristic to $MgAl_2O_4$. As a result, the main phase of Co/Mg/Al can be due to $MgAl_2O_4$-like one (Fig. 3b–d). The diffraction peak of $MgAl_2O_4$ on the Co/Mg/Al catalysts grew first and then disappeared with increasing the (Co + Mg)/Al ratio. On Co/Mg/Al ((Co + Mg)/Al ≥ 1) (Fig. 3d–g), peaks similar to MgO periclase [87] were observed. Considering the Co and Al species are present, MgO solid solution containing Co and Al can be formed and these peaks were assigned to MgO-based solid solution [58]. Comparisons with the XRD patterns of Co/Mg/Al (Fig. 3e–g) and Co/Mg (Fig. 3h) after calcination showed that the diffraction peaks of the Co/Mg/Al were broader than those of Co/Mg, suggesting smaller crystallite of the hydrotalcite-derived oxides, and this tendency agreed well with the previous report for Mg/Al mixed oxide obtained from hydrotalcite precursor [88]. The behavior is connected to the larger BET surface area of the Co/Mg/Al samples (89–92 m^2/g-cat) than that of Co/Mg (28 m^2/g-cat) (Table 2), indicating that the presence of Al^{3+} suppresses the sintering of oxides.

Fig. 4 shows the TPR profiles of the calcined samples of Co/Mg/Al, Co/α-Al_2O_3, Co/Al and Co/Mg. The reduction of Co species on Co/α-Al_2O_3 proceeded in narrow temperature range of 473–773 K. According to our previous report [36], the amount of H_2 consumption of Co/α-Al_2O_3 (12 wt% Co, 2.1 mmol Co/g-cat) was determined to be 2.9 mmol/g-cat, and the reduction degree of Co was calculated to be 1.0 assuming $Co_3O_4 + 4H_2 \rightarrow 3Co + 4H_2O$. On the other hand, the reduction of Co/Al occurred mainly around 1253 K, which was very higher than the case of Co/α-Al_2O_3. This behavior is related to the property of the Co species of Co/Al, which can be assigned to $CoAl_2O_4$ observed by XRD (Fig. 3a). The lower reducibility of $CoAl_2O_4$ than Co_3O_4 is also supported by the previous report [89] and low reducibility of metal ions in $MgAl_2O_4$-based structure has been also observed in the case of Ni [90]. All of Co/Mg/Al catalysts showed a clear reduction peak with a maximum at high temperature region of 1133–1253 K, which is attributed to the reduction of Co species in MgO- and $MgAl_2O_4$-based solid solutions observed in the XRD results (Fig. 3). For the Co/Mg/Al catalysts with (Co + Mg)/Al ≤ 1, the H_2 consumption peak on Co/Mg/Al is shifted gradually to lower temperature with increasing the Mg content. In contrast, for the Co/Mg/Al catalysts with ((Co + Mg)/Al ≥ 1), the H_2 consumption peak on Co/Mg/Al is shifted gradually to higher

Table 2
Physicochemical properties of the catalysts after calcination and reduction.

Entry	Catalysts	BET surface area (m^2/g-cat)[a]	O_2 consumption in TPO (mmol/g-cat)	Co reduction degree (%)[b]	H_2 adsorption (10^{-6} mol/g)[c]	Dispersion of Co metal (H_2 adsorption) (%)[d]	Size of Co particles (nm)	
							H_2 adsorption[e]	XRD[f]
1	Co/Al	125	0.7	51	21	4.0	24	12
2	Co/Mg/Al (10/10/80)	119	0.4	29	13	4.4	22	10
3	Co/Mg/Al (10/23/67)	110	0.5	37	20	5.3	18	10
4	Co/Mg/Al (10/40/50)	100	1.1	81	32	3.9	25	7
5	Co/Mg/Al (9/57/33)	92	1.2	88	36	4.0	24	8
6	Co/Mg/Al (9/66/25)	91	0.5	37	26	6.9	14	8
7	Co/Mg/Al (9/74/17)	89	0.4	29	19	6.4	15	8
8	Co/Mg	28	0.2	15	1.8	1.2	82	–

[a] After the calcination.
[b] Calculated from the temperature programmed oxidation measurement of the reduced catalysts (Fig. 5). Co reduction degree (%) = (the O_2 consumption in TPO)/(Co amount/58.9/3 × 2) × 100.
[c] The total adsorption (Irreversible + Reversible) at room temperature at the catalysts after reduction.
[d] Dispersion of Co metal particles: 2 × (H_2 uptake)/(Co reduction degree × Co amount/58.9) × 100%, assuming H/Co = 1.
[e] Calculated using the equation: d (nm) = 9.63/(dispersion %) × 10 [42].
[f] Fig. 7.

temperature with increasing the Mg content. The TPR profile of Co/Mg showed no obvious peak up to 1273 K, suggesting very low reducibility of the MgO-based solid solution containing Co like the case of Ni species [91–93]. The reduction behavior of Co/Mg/Al catalysts was different from that of Co/Mg as mentioned above. The presence of Al^{3+} can promote the reduction of Co^{2+} and Co^{3+}, and the higher reducibility of Co/Mg/Al samples compared to that of Co/Mg catalyst is probably due to the incorporation of Al^{3+} in the MgO-based structure. It is also interpreted that the presence of Al^{3+} in the solid solution suppresses the crystallite growth, enhances the BET surface area (Table 2), thus the amount of reducible ion species located at the position, where the reducing agent (H_2) is accessible, is increased [59]. As a result, the reduction temperature higher than 973 K is necessary because the active species for the steam reforming reaction is Co metal. The amount of Co metal can be increased with increasing the reduction temperature. However, too severe reduction condition can cause the aggregation of metal particles. Therefore, the medium reduction condition should be adopted. Based on the previous report on Ni/Mg/Al [59], the present reduction condition (1073 K, H_2/N_2 = 30/30 ml/min) were used for the reduction pretreatment, here, the reduction degree of Co on Co/Mg/Al cannot be as high as that of Co/α-Al_2O_3. However, it is impossible to estimate the reduction degree only from the results of TPR profiles. Therefore, we measured the TPO profiles of the catalysts after the reduction pretreatment.

Fig. 5 shows the TPO profiles of Co/Al, Co/Mg and Co/Mg/Al catalysts. The O_2 consumption peak due to the oxidation of Co metal was observed with a maximum at 530–700 K, where it is interpreted that Co metal particles are oxidized to Co_3O_4 according to the previous report [78]. Therefore, the reduction degree was calculated from the O_2 consumption assuming this stoichiometry of the oxidation of Co metal to Co_3O_4 and the results are also listed in Table 2. For Co/Mg/Al ((Co + Mg)/Al ≤ 2) catalysts, the Co reduction degree increased from 29% to 88% with increasing the Mg content (Table 2, entries 1–5), On Co/Mg/Al ((Co + Mg)/Al ≥ 2) catalysts, the Co reduction degree decreased from 88% to 29% with further increase of the Mg content (Table 2, entries 5–7). It should be noted that this tendency was essentially in agreement with the order of the catalyst reducibility observed from TPR measurements (Fig. 4).

The amount of H_2 adsorption was measured and the results are also listed in Table 2. It is possible to calculate the dispersion of Co metal using the Co reduction degree and the H_2 adsorption amount (Table 2). In addition, the average metal particle size was also calculated by the obtained dispersion of Co metal and it is also listed in Table 2. In order to confirm the metal particle size, we also observed the reduced Co/Mg/Al (10/40/50) by TEM. Fig. 6 shows the TEM image of Co/Mg/Al (10/40/50) and the size distribution of Co metal particles. The averaged size of Co metal particles was estimated to be 14 nm, which is smaller than that from the H_2 adsorption amount (25 nm, Table 2, entry 4). This behavior can be explained by the partial coverage of Co metal surface with oxides, and the similar phenomenon has been also observed in the case of Ni/Mg/Al [59] and metal particles modified with oxide clusters [94,95]. The BET surface area of Co/Mg/Al (10/40/50) after the reduction pretreatment was measured to be 108 m^2/g. Assuming that the oxides in the reduced Co/Mg/Al can be $MgAl_2O_4$, the size of the crystallite is calculated to be 15.6 nm, which is comparable to the size of Co metal particles (14 nm from TEM). The Co/Mg/Al (10/40/50) has a nanocomposite structure consisted of Co metal particles (14 nm) and $MgAl_2O_4$-based solid solution particles (~16 nm). The formation of nanocomposite structure can enhance the interface between the metal and the oxide, and at the same time, the interaction between the metal and the oxide can decrease the surface area of the Co metal particles by partial covering with the oxides. This

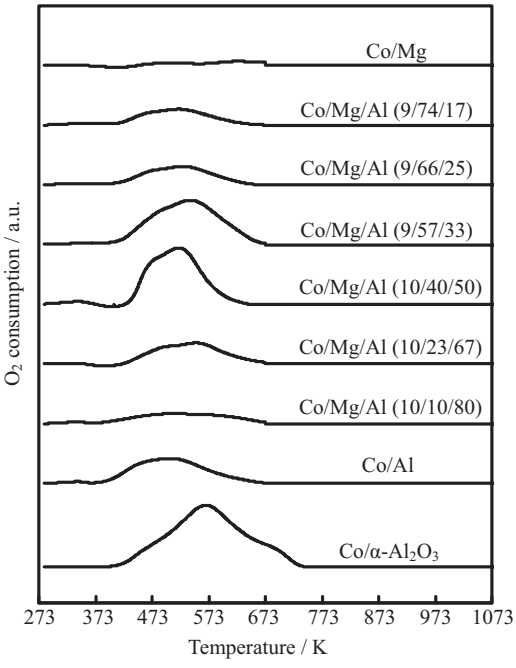

Fig. 5. TPO profiles of Co/Mg, Co/Al and Co/Mg/Al catalysts. TPO conditions: heating rate 10 K/min, 1% O_2/He flow rate 30 ml/min. Sample weight: 50 mg.

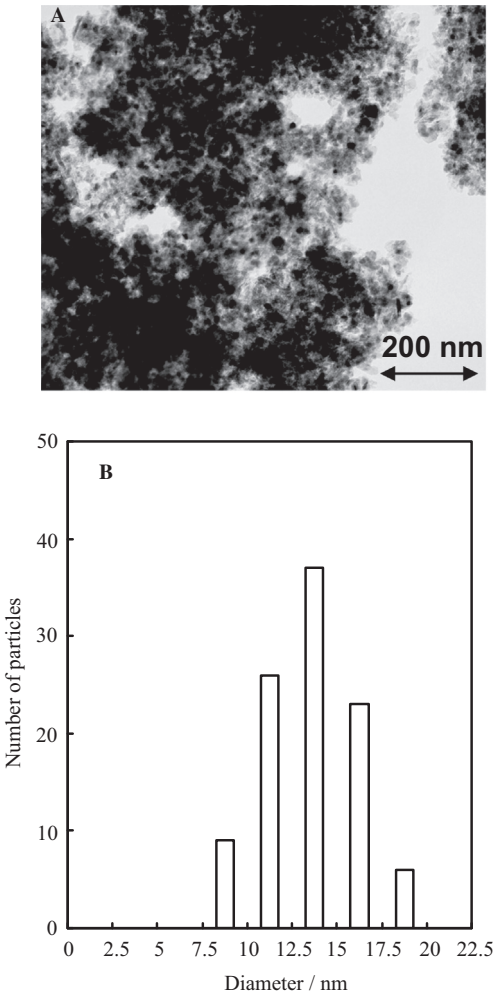

Fig. 6. TEM image of the Co/Mg/Al ((Co + Mg)/Al = 1) (A) and the distribution of the size of Co metal particles (B) after H_2 pretreatment at 1073 K.

interpretation can explain that the particle size estimated from H_2 adsorption is larger than that of TEM.

Fig. 7 shows the XRD patterns of Co/Al, Co/Mg and Co/Mg/Al after the reduction pretreatment. The peak due to Co metal was observed at $2\theta = 51.5^\circ$ on Co/Mg/Al [96], and the analysis of the peak broadening gave the size of Co metal particles (Table 2). The Co metal particle size from XRD is smaller than that from TEM. In

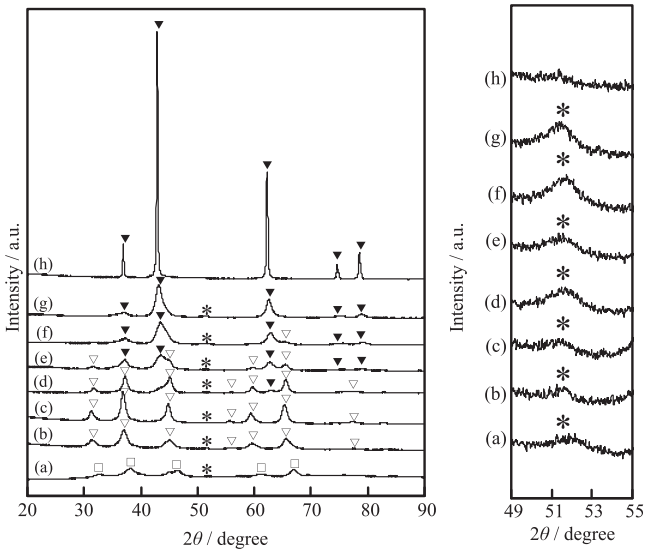

Fig. 7. XRD patterns of the samples after reduction at 1073 K for 30 min in the H_2/N_2 mixed gas: (a) Co/Al, (b) Co/Mg/Al (10/10/80), (c) Co/Mg/Al (10/23/67), (d) Co/Mg/Al (10/40/50), (e) Co/Mg/Al (9/57/33), (f) Co/Mg/Al (9/66/25), (g) Co/Mg/Al (9/74/17) and (h) Co/MgO. ▼ = MgO-based solid solution, ▽ = $MgAl_2O_4$-based solid solution, □ = $CoAl_2O_4$ spinel and * = Co metal.

order to elucidate the reason for the disagreement in the metal particle sizes, further investigation is necessary. At present, it is thought that one Co metal particle (14 nm) can consist of some smaller crystallites (7 nm) on the Co/Mg/Al (10/40/50) catalyst.

3.2. Catalytic performance of Co/Mg/Al in the steam gasification of biomass

Fig. 8 shows the catalytic performance of Co/α-Al_2O_3, Co/Al, Co/Mg/Al and Co/Mg in steam gasification of biomass at 823 K. In the case of Co/α-Al_2O_3, the amount of the residual tar was large and the ratio of H_2 to CO (H_2/CO) was rather low, indicating the low catalytic activity of Co/α-Al_2O_3 in the steam reforming reaction of tar derived from the pyrolysis of cedar wood. In contrast, Co/Al catalyst showed higher steam gasification activity than Co/α-Al_2O_3. On the other hand, the addition of Mg to Co/Al decreased the amount of tar in the range of the molar ratio of (Co + Mg)/Al ≤ 1, and this means the addition of Mg to Co/Al promoted the steam gasification reaction monotonously in the range of the molar ratio of (Co + Mg)/Al ≤ 1, and the amount of tar decreased. In contrast,

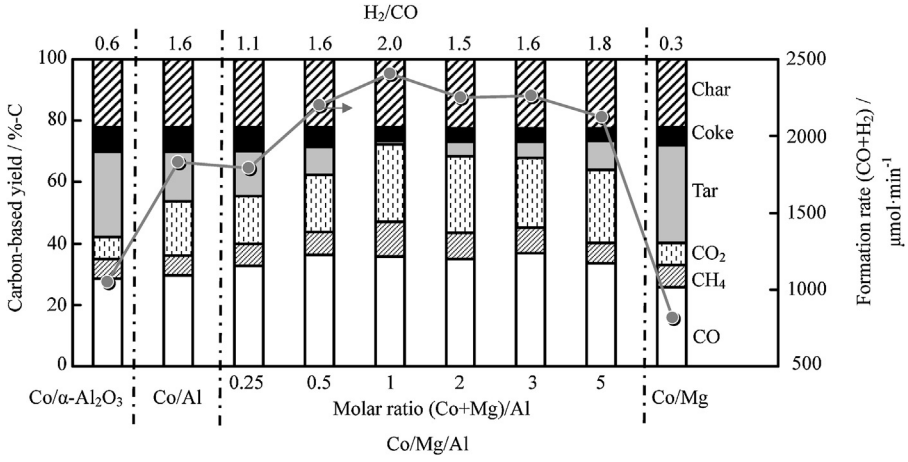

Fig. 8. Catalytic performance in steam gasification of biomass over Co/α-Al_2O_3, Co/Al, Co/Mg. and Co/Mg/Al catalysts at 823 K. Catalyst weight was 0.3 g, S/C = 0.47.

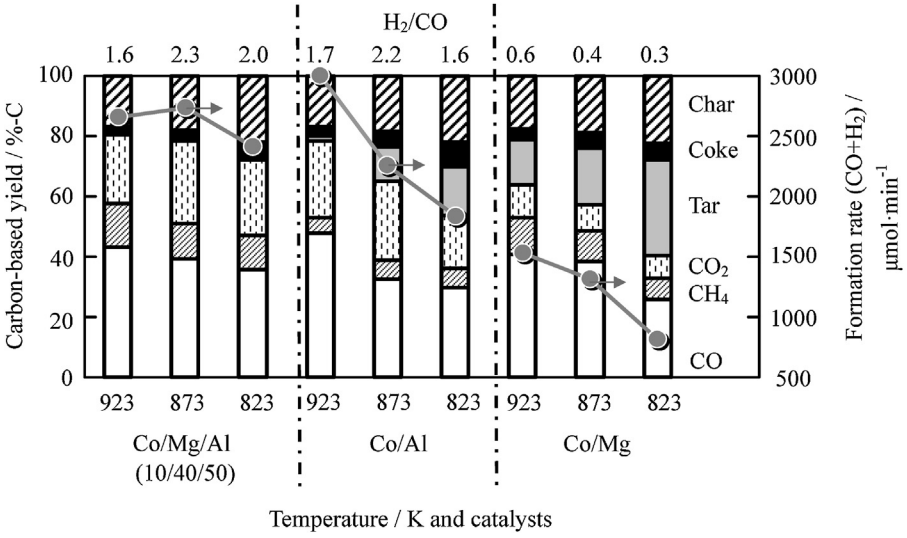

Fig. 9. Reaction temperature dependence on steam gasification of biomass over Co/Mg, Co/Al. and Co/Mg/Al (10/40/50) after H2 reduction. Catalyst weight was 0.3 g, S/C = 0.47.

the excess addition of Mg ((Co + Mg)/Al ≤ 1) decreased the formation rate of gaseous products significantly and increased the tar amount. The catalytic performance of Co/Mg/Al in the steam gasification, which is reflected by the tar amount, is highest on Co/Mg/Al (10/40/50) ((Co + Mg)/Al = 1). It should be noted that Co/Mg exhibited very low activity, under the present reaction condition, although MgO-supported catalysts have been reported to be effective to the tar removal [51]. The behavior is similar to the dependence of the catalytic performance in the steam gasification on the additive amount of Mg over Ni/Mg/Al in the previous report [35]. The activity of the steam gasification can be strongly dependent on the number of surface Co atoms and the H_2 adsorption amount. The H_2 adsorption amount of Co/α-Al_2O_3 was measured to be 30 μmol/g-cat [36]. The Co/Al has smaller amount of H_2 adsorption, however, the activity of Co/Al was higher than that of Co/α-Al_2O_3. This suggests that Co metals on $CoAl_2O_4$ and γ-Al_2O_3 exhibits higher turnover frequency than those on α-Al_2O_3. The H_2 adsorption amount of Co/Mg/Al was comparable to that of Co/α-Al_2O_3 and Co/Al, in contrast, Co/Mg/Al exhibited clearly higher activity, in particular, Co/Mg/Al (10/40/50) and Co/Mg/Al (9/57/33). This results suggest that high activity is caused by the interaction between Co metal particles and the support materials of MgO- and $MgAl_2O_4$-based solid solution.

Here, we show the H_2 yield in the steam gasification, which is also a key parameter for evaluating the steam reforming of a feed. In the case of Co/Mg/Al ((Co + Mg)/Al = 1, Co/Mg/Al = 10/40/50) in Fig. 8, the formation rate of H_2 was 1623 μmol/min. The total feeding rate of hydrogen in the biomass, its moisture, and the steam is calculated to be 6053 μmol/min. The yield of H_2 is calculated by 2 × (H_2 formation rate)/(total feeding rate of hydrogen), and is determined to be 54%. The H_2 yield is not so high because of the formation of CH_4, coke and char.

Fig. 9 shows the reaction temperature dependence of the catalytic performance in the steam gasification over Co/Mg/Al (10/40/50), Co/Al and Co/Mg. The Co/Mg catalyst showed low activity even at 923 K, and much higher reaction temperature was needed for the total removal of the tar. The Co/Al showed much higher activity and the tar yield became almost zero at 923 K. In the case of Co/Mg/Al (10/40/50), the tar yield was almost zero even at 823 K, indicating higher activity of Co/Mg/Al (10/40/50) than that of Co/Al. The performance of Co/Mg/Al (10/40/50) at 823 K was comparable to that of Co/Al at 873 K, meaning that the reaction temperature can be decreased by the catalyst optimization.

Fig. 10 shows the formation rate of gaseous products as a function of time on stream over Co/Al and Co/Mg/Al (10/40/50) at 873 K. The deactivation of Co/Al was observed clearly after 40 min and the formation rate of H_2 decreased more significantly than that of other products, indicating the decrease of the steam reforming activity. On the other hand, Co/Mg/Al (10/40/50) maintained the activity for 120 min, and it is concluded that Co/Mg/Al (10/40/50) was much more stable than Co/Al. As shown in Fig. S1, the XRD patterns of the catalysts after the catalytic use were almost the same as those after the reduction treatment. The deactivation of Co/Al can be due

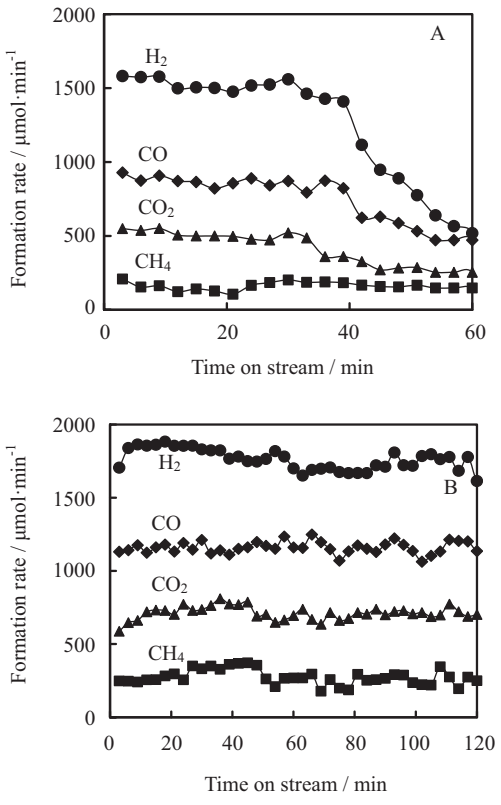

Fig. 10. Reaction time dependence of steam gasification of biomass at 873 K over (A) Co/Al and (B) CoMgAl (10/40/50). Catalyst weight was 0.3 g, S/C = 0.47.

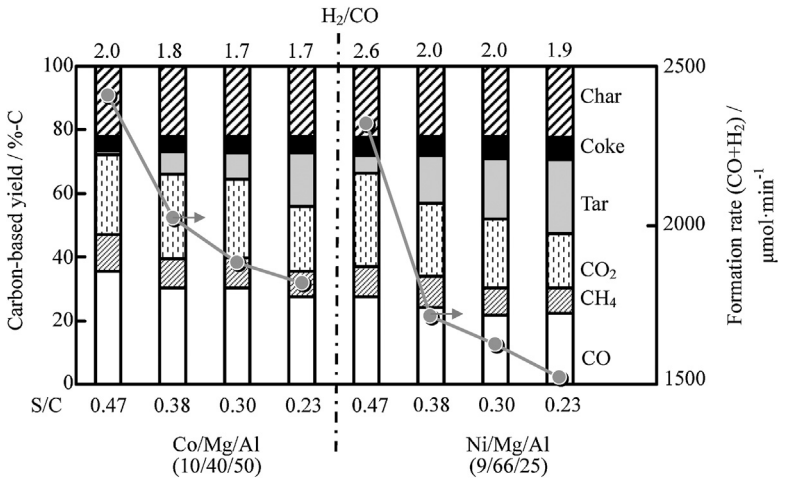

Fig. 11. Catalytic performance in steam gasification of biomass over Co/Mg/Al and Ni/Mg/Al. catalysts at 823 K. Catalyst weight was 0.3 g.

to the coke deposition. The stability test for only 2 h is insufficient from the practical viewpoint. Further investigation is necessary, however, our study on the catalyst development is in progress, and longer stability test will be carried out using a developed catalyst with higher performance.

3.3. Comparison between Co/Mg/Al and Ni/Mg/Al in the steam gasification of biomass

Our group has reported that Ni/Mg/Al prepared from the hydrotalcite-like precursor has high activity in this reaction [59]. Here, the catalytic performance of Co/Mg/Al (10/40/50) was compared with that of the optimized Ni/Mg/Al in our previous work [59], in particular, the reaction tests were carried out at lower S/C ratio in order to make the activity difference clearer.

Fig. 11 shows the catalytic performance of Co/Mg/Al (10/40/50) and Ni/Mg/Al (9/66/25) [59] in steam gasification at 823 K with a series of steam/carbon ratios. Co/Mg/Al (10/40/50) exhibited higher catalytic activity than Ni/Mg/Al (9/66/25). The H_2 adsorption amount of Ni/Mg/Al (9/66/25) was determined to be 43 μmol/g-cat [59], which was larger than that of Co/Mg/Al (10/40/50) (Table 2, entry 4). Considering from the H_2 adsorption amount, Co/Mg/Al was especially superior to Ni/Mg/Al, and the same trend has been also reported on Co/α-Al_2O_3 and Ni/α-Al_2O_3 [36]. These behaviors are connected to the high potential of Co metal as an active species. In the steam gasification in the present reaction temperature range, the biomass was pyrolyzed to the oxygen-containing tar compounds [5], and the catalytic performance can be reflected by the steam reforming activity of the oxygen-containing compounds [51,57,97], and this can explain the difference between Co and Ni.

3.4. Catalyst regeneration test and characterization

It has been known that catalysts can be deactivated by the coke deposition [98–100] and structural change such as the aggregation of metal particles [98] in the reforming reaction. The deactivation becomes severer when the partial pressure ratio of steam to carbon is lower, because of the higher rate of carbon deposition. However, the suppression of coke deposition by higher partial pressure of steam than the reaction stoichiometry decreased the energy efficiency of the steam gasification reaction. One possible method for the energy-efficient steam gasification with an appropriate partial pressure of steam is the development of catalysts with higher resistance to coke deposition. However, it is not easy to suppress the coke formation completely. The regeneration of the used catalyst

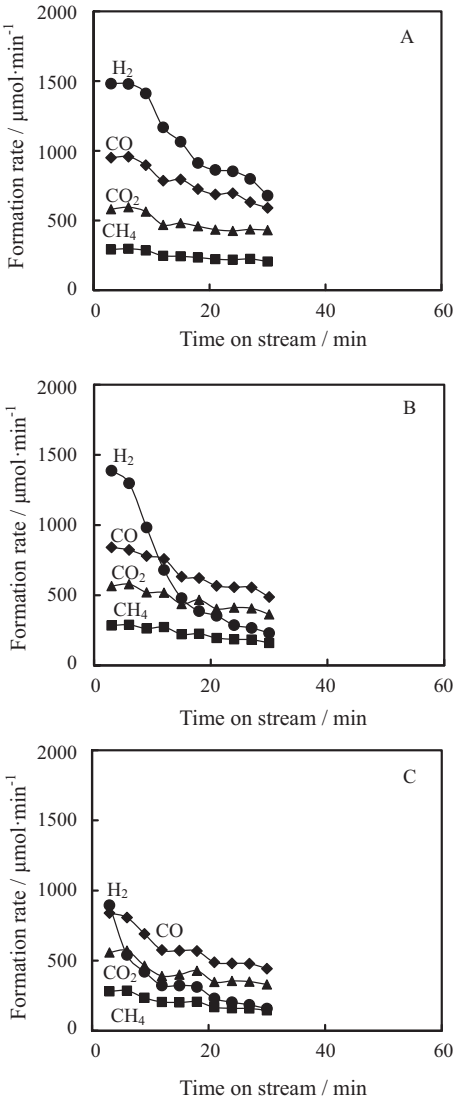

Fig. 12. Reaction time dependence of steam gasification of biomass over Co/α-Al_2O_3 at 873 K and S/C = 0.23. Catalyst weight was 0.3 g. (A) The fresh catalyst reduced at 773 K in H_2. (B) The used catalyst of (A) after the oxidation with O_2/N_2 (1/3) at 873 K for 1 h and the subsequent reduction at 773 K in H_2. (C) The used catalyst of (B) after the oxidation with O_2/N_2 (1/3) at 873 K for 1 h and the subsequent reduction at 773 K in H_2.

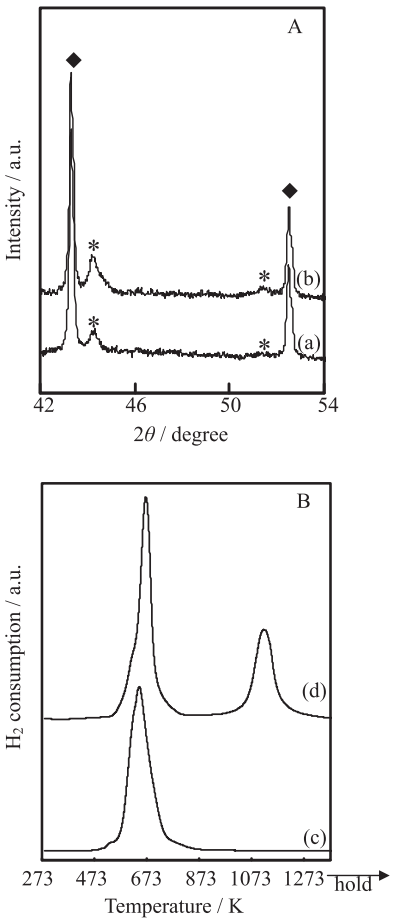

Fig. 13. XRD patterns (A) and TPR profiles (B) of Co/α-Al_2O_3 before and after the catalytic use. (a) Co/α-Al_2O_3 after reduction, (b) Co/α-Al_2O_3 after the reaction (Fig. 12c), (c) Co/α-Al_2O_3 after calcination, (d) the used catalyst of (b) after the oxidation. ♦ = α-Al_2O_3 and * = Co metal.

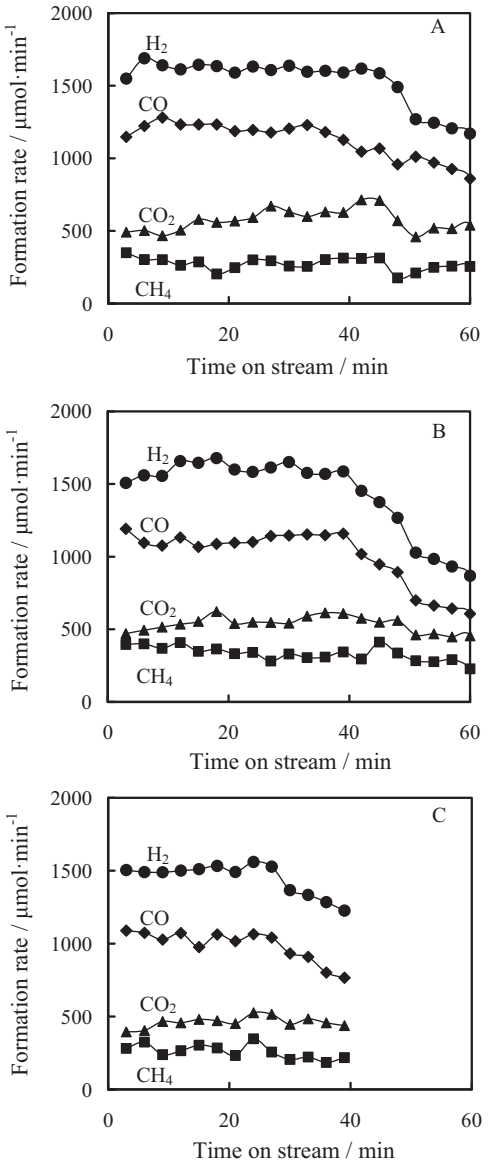

Fig. 14. Reaction time dependence of steam gasification of biomass over Co/Mg/Al (10/40/50) at 873 K and S/C = 0.23. Catalyst weight was 0.3 g. (A) The fresh catalyst reduced at 1073 K in H_2/N_2 (1/1). (B) The used catalyst of (A) after the oxidation with O_2/N_2 (1/3) at 873 K for 1 h and the subsequent reduction at 1073 K in H_2/N_2 (1/1). (C) The used catalyst of (B) after the oxidation with O_2/N_2 (1/3) at 873 K for 1 h and the subsequent reduction at 1073 K in H_2/N_2 (1/1).

by the removal of the deposited coke with the combustion is an important property [101], in particular, in terms of the practical view.

In order to evaluate the deactivation behavior and the regeneration ability, the activity test was carried out at low steam to carbon ratio (S/C = 0.23). Fig. 12 shows the results of the repeated use of Co/α-Al_2O_3 in the steam gasification. At low S/C of 0.23, the catalytic performance of Co/α-Al_2O_3 was rather low. Even on the fresh Co/α-Al_2O_3, the deactivation of the catalyst was very severe. The amount of the deposited carbon after the test of Fig. 12A was determined to be 9.1 mmol/g-cat, indicating that the coke deposition is one of the main causes of the catalyst deactivation. In addition, the activity of Co/α-Al_2O_3 decreased significantly with the repeated times, these results indicate that the regeneration ability of Co/α-Al_2O_3 was low. Fig. 13 shows the characterization result by XRD and TPR of Co/α-Al_2O_3 after the reduction and the catalytic use in Fig. 12, and it is found that the Co metal particle size after the reaction was obtained to be 34 nm (Fig. 13b), which was larger than that of freshly reduced Co/α-Al_2O_3 catalyst (25 nm). The low regeneration ability of Co/α-Al_2O_3 is interpreted by the aggregation of the metal particles during the reaction and regeneration procedure. At the same time, the TPR profile of Co/α-Al_2O_3 after the catalytic use and subsequent oxidation treatment gave two kinds of H_2 consumption peak. The lower temperature peak was observed at the similar position on fresh Co/α-Al_2O_3, however, the peak become a little sharper. On both catalysts, this kind of peak can be assigned to the reduction of Co_3O_4 [102]. On the other hand, the used Co/α-Al_2O_3 gave higher temperature peak (~1125 K), and this peak can be assigned to the reduction of $CoAl_2O_4$ [102]. During the regeneration procedure, the solid phase reaction between Co oxide and α-Al_2O_3 can proceed. The solid phase reaction can be connected to the decrease in catalytic activity through the decrease in the reduction degree of Co species. Totally, the aggregation of Co metal species and the formation of Co species with lower reducibility are the cause of the catalyst deactivation in the repeated use.

Fig. 14 shows the results of the repeated use of Co/Mg/Al (10/40/50) in the steam gasification. Even at low S/C conditions, Co/Mg/Al (10/40/50) maintained much higher activity of the steam gasification than Co/α-Al_2O_3. The amount of deposited coke was 3.0 mmol/g-cat after 60 min (Fig. 14A), which was smaller than that on Co/α-Al_2O_3 (Fig. 12A). This means that Co/Mg/Al can keep high activity on the catalyst. On the other hand, the steam gasification activity of Co/Mg/Al (10/40/50) gradually decreased by the repeated times, although the decrease was much smaller than that

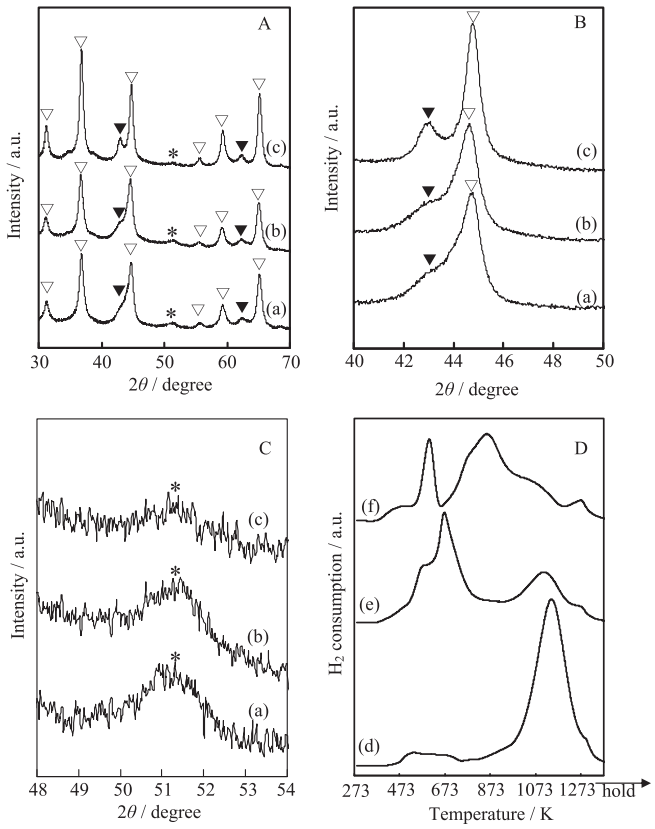

Fig. 15. XRD patterns (A, B, C) and TPR patterns (D) of the Co/Mg/Al (10/40/50) before and after the catalytic use. (a) Co/Mg/Al (10/40/50) after reduction, (b) Co/Mg/Al (10/40/50) after the reaction (Fig. 13a), (c) Co/Mg/Al (10/40/50) after the reaction (Fig. 13c), (d) Co/Mg/Al (10/40/50) after calcination, (e) Co/Mg/Al (10/40/50) after reduction and the subsequent oxidation, (f) the used catalyst of (c) after the oxidation. ▼ = MgO-based solid solution, ▽ = $MgAl_2O_4$-based solid solution and * = Co metal.

of Co/α-Al_2O_3. In addition, the regeneration ability of Co/Mg/Al (10/40/50) was also superior to that of Ni/Mg/Al (9/66/25) as shown in Fig. S2.

Fig. 15 shows the XRD patterns and TPR profiles of Co/Mg/Al (10/40/50) before and after the catalytic use. It is characteristic that the peak around $2\theta = 43^\circ$ grew with increasing with the usage times. This peak is assigned to MgO-based solid solution. In addition, the TPR profile on Co/Mg/Al after the oxidation of the used catalyst was different from that of freshly calcined Co/Mg/Al. This difference can be due to the Co metal formation by the reduction pretreatment. Therefore, we also measured the TPR profile of fresh Co/Mg/Al after the reduction and the subsequent oxidation (Fig. 15e). On this sample, the main hydrogen consumption peak was observed in the range of 473–773 K. This can be due to the reduction of Co_3O_4 which is formed by the oxidation of Co metal on the freshly reduced Co/Mg/Al. The reduction degree of Co below 1073 K is calculated to be 62%. In the case of the Co/Mg/Al catalyst after the catalytic use followed by the oxidation, the hydrogen consumption peak in the medium temperature range (673–1073 K) grew significantly, which is not observed in the present work. Judging from the XRD patterns of Fig. 15B, the repeated use changed the structure of oxides to give MgO-based solid solution. The temperature of hydrogen consumption peak of the Co species in the MgO-based solid solution was much higher as shown in Fig. 4. An important point is that the oxidation temperature for the catalyst regeneration (873 K) was much lower than the calcination for the catalyst preparation (1073 K). Therefore, the oxidized Co species at 873 K cannot diffuse into the bulk of oxides, but to the near surface of the oxides. In this case, the concentration of the Co species at the near surface can be rather high and connected to higher reducibility. The reduction degree of Co in Fig. 15f below 1073 K is calculated to be 67%. On the other hand, the XRD peak due to Co metal (Fig. 15C(c)) was weaker and broader than those of other samples. This tendency suggests the increase of Co metal dispersion during the catalytic use. Relating to the lower activity of the catalyst after the three-time repeated use, these Co metal particles with higher dispersion loaded on MgO-based solid solution can show lower activity than Co metal particles with lower dispersion on $MgAl_2O_4$-based solid solution.

4. Conclusions

1. In the steam gasification of cedar wood, the Co/Mg/Al catalyst prepared from hydrotalcite-like precursor with suitable composition (Co/Mg/Al = 10/40/50) exhibited higher activity and higher resistance to coke deposition than Co/α-Al_2O_3, Co/Al and Co/Mg catalysts.
2. The Co/Mg/Al (10/40/50) catalyst exhibited higher catalytic performance than the Ni/Mg/Al (9/66/25) catalyst in terms of the activity and the regeneration ability of the deactivated catalysts.
3. From the results of the catalyst characterization, the Co/Mg/Al (10/40/50) catalyst after the reduction pretreatment has a nanocomposite structure of the Co metal particles (~14 nm) and the oxide particles (~16 nm) of $MgAl_2O_4$-based solid solution. The composite structure can be connected to high catalytic performance such as high resistance to coke deposition by the metal-oxide interaction and the suppression of the aggregation of Co metal particles.
4. In order to improve the property of Co/Mg/Al (10/40/50) in the repeated catalyst regeneration by the coke removal with the combustion and the subsequent catalyst activation by the reduction treatment, the structural change of $MgAl_2O_4$-based solid solution to MgO-based solid solution should be avoided.

Acknowledgement

This work was supported by the Cabinet Office, Government of Japan through its "Funding Program for Next Generation World-Leading Researchers".

Appendix A. Supplementary data

Supplementary data associated with this article can be found, in the online version, at http://dx.doi.org/10.1016/j.apcatb.2013.12.002.

References

[1] G.W. Huber, S. Iborra, A. Corma, Chem. Rev. 106 (2006) 4044.
[2] D. Li, Y. Nakagawa, K. Tomishige, Chin. J. Catal. 33 (2012) 583.
[3] D. Li, L. Wang, M. Koike, K. Tomishige, J. Jpn. Petrol. Inst. 56 (2013) 253.
[4] A.V. Bridgwater, Appl. Catal. A: Gen. 116 (1994) 5.
[5] H. de Lasa, E. Salaices, J. Mazumder, R. Lucky, Chem. Rev. 111 (2011) 5404.
[6] S. Sá, H. Silva, L. Brandão, J.M. Sousa, A. Mendes, Appl. Catal. B: Environ. 99 (2010) 43.
[7] M.M. Yung, W.S. Jablonski, K.A. Magrini-Bair, Energy Fuels 23 (2009) 1874.
[8] K. Tomishige, M. Asadullah, K. Kunimori, Catal. Today 89 (2004) 389.
[9] C. Xu, J. Donald, E. Byambajav, Y. Ohtsuka, Fuel 89 (2010) 1784.
[10] T. Furusawa, A. Tsutsumi, Appl. Catal. A: Gen. 278 (2005) 195.
[11] C. Pfeifer, R. Rauch, H. Hofbauer, Ind. Eng. Chem. Res. 43 (2004) 1634.
[12] D. Świerczyński, S. Libs, C. Courson, A. Kiennemann, Appl. Catal. B: Environ. 74 (2007) 211.
[13] J.N. Kuhn, Z. Zhao, A. Senefeld-Naber, L.G. Felix, R.B. Slimane, C.W. Choi, U.S. Ozkan, Appl. Catal. A: Gen. 341 (2008) 43.
[14] E.G. Baker, L.K. Mudge, M.D. Brown, Ind. Eng. Chem. Res. 26 (1987) 1335.
[15] M. Asadullah, T. Miyazawa, S. Ito, K. Kunimori, K. Tomishige, Appl. Catal. A: Gen. 246 (2003) 103.
[16] M. Asadullah, T. Miyazawa, S. Ito, K. Kunimori, M. Yamada, K. Tomishige, Appl. Catal. A: Gen. 267 (2004) 95.

[17] M. Asadullah, T. Miyazawa, S. Ito, K. Kunimori, M. Yamada, K. Tomishige, Appl. Catal. A: Gen. 255 (2003) 169.
[18] M. Asadullah, S. Ito, K. Kunimori, M. Yamada, K. Tomishige, Environ. Sci. Technol. 36 (2002) 4476.
[19] W. Cai, P.R. de la Piscina, N. Homs, Appl. Catal. B: Environ. 145 (2014) 56.
[20] S. Weng, Y. Wang, C. Lee, Appl. Catal. B: Environ. 134–135 (2013) 359.
[21] B. Matas Güell, I. Babich, K.P. Nichols, J.G.E. Gardeniers, L. Lefferts, K. Seshan, Appl. Catal. B: Environ. 90 (2009) 38.
[22] X. Hu, G. Lu, Appl. Catal. B: Environ. 99 (2010) 289.
[23] D.A. Constantinou, M.C. Álvarez-Galván, J.L.G. Fierro, A.M. Efstathiou, Appl. Catal. B: Environ. 117–118 (2012) 81.
[24] M. Araque, L.M.T. Martínez, J.C. Vargas, M.A. Centeno, A.C. Roger, Appl. Catal. B: Environ. 125 (2012) 556.
[25] I. Zamboni, C. Courson, D. Niznansky, A. Kiennemann, Appl. Catal. B: Environ. 145 (2014) 63.
[26] J. Li, J. Liu, S. Liao, R. Yan, Int. J. Hydrogen Energy 35 (2010) 7399.
[27] T. Wang, J. Chang, X. Cui, Q. Zhang, Y. Fu, Fuel Process. Technol. 87 (2006) 421.
[28] A. Corujo, L. Yermán, B. Arizaga, M. Brusoni, J. Castiglioni, Biomass Bioenergy 34 (2010) 1695.
[29] K. Tomishige, T. Kimura, J. Nishikawa, T. Miyazawa, K. Kunimori, Catal. Commun. 8 (2007) 1074.
[30] T. Kimura, T. Miyazawa, J. Nishikawa, S. Kado, K. Okumura, T. Miyao, S. Naito, K. Kunimori, K. Tomishige, Appl. Catal. B: Environ. 68 (2006) 160.
[31] J. Nishikawa, K. Nakamura, M. Asadullah, T. Miyazawa, K. Kunimori, K. Tomishige, Catal. Today 131 (2008) 146.
[32] J. Nishikawa, T. Miyazawa, K. Nakamura, M. Asadullah, K. Kunimori, K. Tomishige, Catal. Commun. 9 (2008) 195.
[33] K. Nakamura, T. Miyazawa, T. Sakurai, T. Miyao, S. Naito, N. Begum, K. Kunimori, K. Tomishige, Appl. Catal. B: Environ. 86 (2009) 36.
[34] M. Koike, C. Ishikawa, D. Li, L. Wang, Y. Nakagawa, K. Tomishige, Fuel 103 (2013) 122.
[35] L. Wang, D. Li, M. Koike, S. Koso, Y. Nakagawa, Y. Xu, K. Tomishige, Appl. Catal. A: Gen. 392 (2011) 248.
[36] L. Wang, D. Li, M. Koike, H. Watanabe, Y. Xu, Y. Nakagawa, K. Tomishige, Fuel 112 (2013) 654.
[37] M. Koike, D. Li, Y. Nakagawa, K. Tomishige, ChemSusChem 5 (2012) 2312.
[38] J. Ashok, S. Kawi, Int. J. Hydrogen Energy 38 (2013) 13938.
[39] U. Oemar, P.S. Ang, K. Hidajat, S. Kawi, Int. J. Hydrogen Energy 38 (2013) 5525.
[40] B. Valle, B. Aramburu, A. Remiro, J. Bilbao, A.G. Gayubo, Appl. Catal. B: Environ. 147 (2014) 402.
[41] G. Garbarino, E. Finocchio, A. Lagazzo, I. Valsamakis, P. Riani, V.S. Escribano, G. Busca, Appl. Catal. B: Environ. 147 (2014) 813.
[42] F. Bimbela, D. Chen, J. Ruiz, L. García, J. Arauzo, Appl. Catal. B: Environ. 119–120 (2012) 1.
[43] B. Matas Güell, I.V. Babich, L. Lefferts, K. Seshan, Appl. Catal. B: Environ. 106 (2011) 280.
[44] G. Guan, G. Chen, Y. Kasai, E.W.C. Lim, X. Hao, M. Kaewpanha, A. Abuliti, C. Fushimi, A. Tsutsumi, Appl. Catal. B: Environ. 115–116 (2012) 159.
[45] G. Garbarino, V. Sanchez Escribano, E. Finocchio, G. Busca, Appl. Catal. B: Environ. 113–114 (2012) 281.
[46] J. Remón, J.A. Medrano, F. Bimbela, L. García, J. Arauzo, Appl. Catal. B: Environ. 132–133 (2013) 433.
[47] K. Tasaka, T. Furusawa, A. Tsutsumi, Energy Fuels 21 (2007) 590.
[48] K. Tasaka, T. Furusawa, A. Tsutsumi, Chem. Eng. Sci. 62 (2007) 5558.
[49] D. Li, C. Ishikawa, M. Koike, L. Wang, Y. Nakagawa, K. Tomishige, Int. J. Hydrogen Energy 38 (2013) 3572.
[50] L. Wang, Y. Hisada, M. Koike, D. Li, H. Watanabe, Y. Nakagawa, K. Tomishige, Appl. Catal. B: Environ. 121–122 (2012) 95.
[51] T. Furusawa, A. Tsutsumi, Appl. Catal. A: Gen. 278 (2005) 207.
[52] M. Koike, Y. Hisada, L. Wang, D. Li, H. Watanabe, Y. Nakagawa, K. Tomishige, Appl. Catal. B: Environ. 140–141 (2013) 652.
[53] K. Urasaki, K. Tokunaga, Y. Sekine, M. Matsukata, E. Kikuchi, Catal. Commun. 9 (2008) 600.
[54] A. Kazama, Y. Sekine, K. Oyama, M. Matsukata, E. Kikuchi, Appl. Catal. A: Gen. 383 (2010) 96.
[55] Y. Sekine, A. Kazama, Y. Izutsu, M. Matsukata, E. Kikuchi, Catal. Lett. 132 (2009) 329.
[56] N. Iwasa, S. Masuda, N. Takezawa, React. Kinet. Catal. Lett. 55 (1995) 349.
[57] X. Hu, G. Lu, J. Mol. Catal. A: Chem. 261 (2007) 43.
[58] F. Cavani, F. Trifirò, A. Vaccari, Catal. Today 11 (1991) 173.
[59] D. Li, L. Wang, M. Koike, Y. Nakagawa, K. Tomishige, Appl. Catal. B: Environ. 102 (2011) 528.
[60] S. Miyata, Clays Clay Miner. 23 (1975) 369.
[61] H.F.W. Taylor, Mineral. Mag. 39 (1973) 377.
[62] S. Miyata, A. Okada, Clays Clay Miner. 25 (1977) 14.
[63] S. Miyata, Clays Clay Miner. 31 (1983) 305.
[64] A. Clearfield, Chem. Rev. 88 (1988) 125.
[65] S.P. Newman, W. Jones, N. J. Chem. 22 (1998) 105.
[66] A.L. McKenzie, C.T. Fishel, R.J. Davis, J. Catal. 138 (1992) 547.
[67] C. Busetto, G. Del Piero, G. Manara, F. Trifirò, A. Vaccari, J. Catal. 85 (1984) 260.
[68] R. Espinal, E. Taboada, E. Molins, R.J. Chimentao, F. Medina, J. Llorca, Appl. Catal. B: Environ. 127 (2012) 59.
[69] R. Espinal, E. Taboada, E. Molins, R.J. Chimentao, F. Medina, J. Llorca, RSC Adv. 2 (2012) 2946.
[70] L.C. Meher, R. Gopinath, S.N. Naik, A.K. Dalai, Ind. Eng. Chem. Res. 48 (2009) 1840.
[71] E. Palomares, A. Uzcátegui, C. Franch, A. Corma, Appl. Catal. B: Environ. 142–143 (2013) 795.
[72] J.J. Yu, Z. Jiang, L. Zhu, Z.P. Hao, Z.P. Xu, J. Phys. Chem. B 110 (2006) 4291.
[73] A.E. Palomares, J.M. López-Nieto, F.J. Lázaro, A. López, A. Corma, Appl. Catal. B: Environ. 20 (1999) 257.
[74] J. Pérez-Ramı′rez, J. Overeijnder, F. Kapteijn, J.A. Moulijn, Appl. Catal. B: Environ. 23 (1999) 59.
[75] C. Gennequin, R. Cousin, J.F. Lamonier, S. Siffert, A. Aboukaïs, Catal. Commun. 9 (2008) 1639.
[76] Z. Jiang, J. Yu, J. Cheng, T. Xiao, M.O. Jones, Z. Hao, P.P. Edwards, Fuel Process. Technol. 91 (2010) 97.
[77] C. Gennequin, S. Siffert, R. Cousin, A. Aboukaïs, Top. Catal. 52 (2009) 482.
[78] R.C. Reuel, C.H. Bartholomew, J. Catal. 85 (1984) 63.
[79] M.K. Niemelä, L. Backman, A.O.I. Krause, T. Vaara, Appl. Catal. A: Gen. 156 (1997) 319.
[80] J.T.E. Whyte, Catal. Rev. 8 (1973) 117.
[81] X-Ray Powder Diffraction Data File, ICSD 59609.
[82] X-Ray Powder Diffraction Data File, ICSD 172995.
[83] R. Shannon, Acta Crystallogr. Sect. A: Found. 32 (1976) 751.
[84] X-Ray Powder Diffraction Data File, ICSD 79033.
[85] X-Ray Powder Diffraction Data File, ICSD 77743.
[86] X-Ray Powder Diffraction Data File, ICSD 96837.
[87] X-Ray Powder Diffraction Data File, ICSD 9863.
[88] Z.P. Xu, H.C. Zeng, Chem. Mater. 13 (2001) 4564.
[89] L. Ji, S. Tang, H.C. Zeng, J. Lin, K.L. Tan, Appl. Catal. A: Gen. 207 (2001) 247.
[90] M. Nurunnabi, Y. Mukainakano, S. Kado, T. Miyao, S. Naito, K. Okumura, K. Kunimori, K. Tomishige, Appl. Catal. A: Gen. 325 (2007) 154.
[91] M. Nurunnabi, B. Li, K. Kunimori, K. Suzuki, K. Fujimoto, K. Tomishige, Appl. Catal. A: Gen. 292 (2005) 272.
[92] A. Parmaliana, F. Arena, F. Frusteri, N. Giordano, J. Chem. Soc., Faraday Trans. 86 (1990) 2663.
[93] M. Nurunnabi, Y. Mukainakano, S. Kado, T. Miyazawa, K. Okumura, T. Miyao, S. Naito, K. Suzuki, K. Fujimoto, K. Kunimori, K. Tomishige, Appl. Catal. A: Gen. 308 (2006) 1.
[94] Y. Amada, Y. Shinmi, S. Koso, T. Kubota, Y. Nakagawa, K. Tomishige, Appl. Catal. B: Environ. 105 (2011) 117.
[95] S. Koso, H. Watanabe, K. Okumura, Y. Nakagawa, K. Tomishige, Appl. Catal. B: Environ. 111–112 (2012) 27.
[96] X-Ray Powder Diffraction Data File, ICSD 53805.
[97] N. Iwasa, T. Yamane, M. Takei, J. Ozaki, M. Arai, Int. J. Hydrogen Energy 35 (2010) 110.
[98] J. Sehested, Catal. Today 111 (2006) 103.
[99] K. Tomishige, Y. Himeno, Y. Matsuo, Y. Yoshinaga, K. Fujimoto, Ind. Eng. Chem. Res. 39 (2000) 1891.
[100] M. Nurunnabi, Y. Mukainakano, S. Kado, B. Li, K. Kunimori, K. Suzuki, K. Fujimoto, K. Tomishige, Appl. Catal. A: Gen. 299 (2006) 145.
[101] T. Miyazawa, K. Okumura, K. Kunimori, K. Tomishige, J. Phys. Chem. C 112 (2008) 2574.
[102] S. Velu, K. Suzuki, M.P. Kapoor, S. Tomura, F. Ohashi, T. Osaki, Chem. Mater. 12 (2000) 719.